ELSEVIER

Physica D 122 (1998) 254–264

PHYSICA D

Testing for an attractor in the solar wind flow

Wiesław M. Macek [1]

Space Research Centre, Polish Academy of Sciences, Bartycka 18 A, 00-716 Warsaw, Poland

Received 29 October 1997; received in revised form 4 February 1998; accepted 23 February 1998
Communicated by F.H. Busse

Abstract

We analyse a time series of velocity fluctuations of the low-speed stream of the solar wind measured by the Helios spacecraft in the inner heliosphere. We use moving average and singular-value decomposition filters to give a faithful representation of the solar wind nonlinear behaviour. We have supported our previous result that trajectories describing the system in the inertial manifold of phase space can asymptotically approach the attractor of low-dimension. The obtained characteristics of the attractor are significantly different from those of the surrogate data. Thus these results suggest that the inner heliosphere is *nonlinear* and possibly a deterministic chaotic system. © 1998 Elsevier Science B.V.

Keywords: Nonlinear plasma physics; Solar wind; Signal processing; Turbulence

1. Introduction

Chaos is aperiodic long-term behaviour in a deterministic system that exhibits sensitive dependence on initial conditions, e.g., [1]. In the presence of dissipation, trajectories describing long-time evolution of the system in *phase space* may asymptotically approach a closed invariant set that is called an *attractor*. In such a system chaos requires the low-dimensional attractor and deterministic *nonlinear* time evolution. In infinite-dimensional systems or systems with very large dimension it is often the case that one can show that there exists a low-dimensional manifold, the so-called *inertial manifold*, to which the orbit tends and on which the attractor lies [2]. For aperiodic chaotic evolution, the embedding in space of dimension greater than $2D$ should basically give a topologically faithful reconstruction of the D-dimensional attractor [3–5].

In space plasma physics, the idea of chaotic motion on a strange attractor has been tested for the pulsations in radio emissions from the Sun [6], solar activity data [7], and magnetospheric dynamics, e.g., [8,9].

Consider now the inner heliosphere. Since the 1960s it is known that besides electromagnetic radiation, the Sun also radiates charged particles (mainly protons and electrons) forming a solar wind blowing nearly radially outward from the Sun. The solar wind plasma flowing supersonically at roughly constant speed is quite well modelled within the framework of the hydromagnetic theory. This continuous flow has two forms: slow ($\approx 300\,\mathrm{km\,s^{-1}}$) and fast ($\approx 900\,\mathrm{km\,s^{-1}}$) [10]. The fast wind is associated with coronal holes and is relatively uniform and stable, while the slow wind is more turbulent and consequently quite variable in terms of velocities. We limit our study to the

[1] Fax: (4822) 40 3131; e-mail: macek@cbk.waw.pl.

PII S0167-2789(98)00098-0

low-speed stream. In our case the duration of the low-speed stream is much less than the characteristic time of the solar activity, and we do not study how the solar wind depends on the phase of the solar cycle.

The nature of velocity fluctuations is still only poorly known. In addition, a large number of degree of freedom is usually expected for the magnetofluid model of the solar wind. It is likely that the slow solar wind originates from coronal streamers in a coherent fashion [10]. Indication for a low-dimensional attractor in the slow solar wind is given by Macek and Obojska [11–13]. One can expect that the attractor should contain information about the dynamic variations of these streamers. It is also possible that it represents a structure of the time sequence of near-Sun fine-stream tubes. Obviously, further studies are necessary to confirm that indication. If such an attractor actually exists, one can hope to infer information about these complex nonlinear phenomena from the geometrical properties of the attractor without solving complicated hydromagnetic equations describing the system. The importance of this attractor is also strengthened by a possibility of an approximate prediction of the state of the solar wind, which is a main factor controlling the circumplanetary magnetospheres in our Solar System. In this paper we provide further tests for *nonlinearity* and the chaotic attractor in the solar wind data, including a powerful method of singular system (singular-value decomposition or principal component) analysis and statistical surrogate data tests.

In Section 2 we describe the solar wind data and a basic filter we use and summarize the characteristics of the detrended and smoothed data in Table 1. The method of singular system analysis is reviewed and the choice of the model parameters is discussed in Section 3. Application of this method to the attractor reconstruction from the solar wind data is presented in Section 4. In Section 5 we briefly recall the relation of the method of singular system analysis to the standard calculation of the correlation dimension. Section 6 is devoted to the discussion of main results of our calculation of the correlation dimension of the reconstructed attractor. In particular, we show that a better plateau is obtained by using the singular-value decomposition technique of noise reduction. In addition, the calculated dimensions are significantly different from those obtained from the surrogate data. Also, Lyapunov exponents and entropy are briefly considered. Finally, the main conclusions are given in Section 7.

Table 1
Solar wind velocity fluctuations[a] data

Number of data points, N	4514
Sampling time, Δt	40.5 s
Skewness[b], κ_3	0.45
Kurtosis[b], κ_4	−0.17
Minimum frequency	5.5×10^{-6} Hz
Dominant frequency	1.2×10^{-5} Hz
Maximum frequency	1.2×10^{-2} Hz
Relative complexity[c]	0.2
Autocorrelation time[d], t_a	2.6×10^3 s
Correlation dimension[e], D_2	3.7 ± 0.3
Entropy[c,e], $(q = 2)$, K_2	1/3
Largest Lyapunov exponent[c,e], λ_{max}	1/3 − 1/4
Predictability horizon time[c]	2×10^3 s

[a] Slow trends $(349.7+21.74t-96.61t^2$, with t being a fraction of total sample) were subtracted from the original data, $v_i = v(t_i)$, in km s^{-1}, and the data were (8-fold) smoothed using moving averages. The resulting range of data $v_{max} - v_{min} = 53.04$ km s^{-1}.

[b] The third and fourth moments of the distribution function are (with average velocity $\langle v \rangle = 0.02$ km s^{-1} and standard deviation $\sigma = 8.07$ km s^{-1})

$$\kappa_3 = \frac{1}{N}\sum_{i=1}^{N}\left[\frac{v_i - \langle v\rangle}{\sigma}\right]^3, \kappa_4 = \frac{1}{N}\sum_{i=1}^{N}\left[\frac{v_i - \langle v\rangle}{\sigma}\right]^4 - 3.$$

[c] Approximately.

[d] The autocorrelation time t_a is given by $(\langle v(t)v(t+t_a)\rangle - \langle v(t)\rangle^2)/\sigma^2 = e^{-1}$. We take a delay $\tau = 250\Delta t$ slightly larger than the first zero of this function, $212\Delta t$.

[e] For large enough m, a plateau in Fig. 7(a) and (b), see [12], we have a slope ($q = 2$ in Eq. (1)) $D_2 \approx (\log C_m(r))/\log(r)$, where the correlation function is [16]

$$C_m(r) = \frac{1}{n_{ref}}\sum_{i=1}^{n_{ref}}\frac{1}{n - 2n_c - 1} \times \sum_{j=n_c+1}^{n}\theta(r - |\mathbf{X}(t_i) - \mathbf{X}(t_j)|)$$

with $\theta(x)$ being the unit step function; $\mathbf{X}(t_j)$ denotes one of $n = N - (m-1)\tau$ vectors in the m-dimensional embedding space, $n_{ref} = 1000$ is the number of reference points and $n_c = 4$ is the *Theiler* correction [17]. The average slope for $6 \le m \le 10$ is taken as D_2. Similarly, $K_2 \approx \frac{1}{3}\log_2[C_m(r)/C_{m+3}(r)]$ is the $q = 2$ entropy [18] (base 2) in the same units as λ_{max} (bits per data sample), $8 \le m \le 10$.

2. Data

The duration of low-speed streams is limited to about one week. We analyse the Helios data using the radial velocity component, v, measured in the heliosphere near the Sun, at ~ 0.3 astronomical units (AU) [10]. The intervals between data points are $\Delta t = 40.5$ s. We select an interval between the heliospheric current sheet and the interplanetary shock, which are discontinuities in the solar wind plasma, and take the sequence of $N = 4514$ points $v(t_i)$, where $t_{i+1} = t_i + \Delta t$ for $i = 1, \ldots, N$. These raw data of total duration of $N\Delta t \approx 50.8$ h are shown in Fig. 1(a).

A common problem with real data is their lack of stationarity. This shows up as a general trend seen in Fig. 1(a). Naturally, such a slow change may be a part of the dynamical system, but we do not have sufficient number of data points to resolve slowly varying trends. Therefore before a detailed analysis linear and quadratic trends were subtracted from the original data, see the first footnote to Table 1.

Even though the measurements are quite accurate one can often have a dynamical noise. This is a more subtle way the noise might enter the system. Therefore, in order to remove the noise, we have also needed to slightly smooth the data. Surely, filtering can, in general, change the dimension of the attractor (e.g., autoregressive filters, cf. [14]). But we consider a particular finite impulse response (FIR) filter. Namely, we repeatedly replace each data point with the average of itself and its two nearest neighbours. Naturally, volume is invariant under this transformation. More precisely, it can be proved that every generic finite-step moving average filter preserves the correlation dimension, because it preserves the one-to-one property [4]. The conventional wisdom is that applying an FIR filter is like a change of coordinates (finite stretching is Lipschitz). On the contrary, infinite impulse response filter (IIR) may only *increase* the dimension. The latter is equivalent to augmenting the dynamical system with a new variable [15].

Of course, in practice, whether the moving average filter looks like FIR or IIR depends on the number of iterations and the data. In our case this *linear* smoothing procedure is reasonably well converged after several steps and eight iterations are sufficient. Thus, what is remaining should represent a nonlinear dynamics of the system. At worse, this procedure can only *increase* the actual dimension [14]. Hence the smoothed data should give a faithful representation of the attractor. The detrended data remaining after this procedure are shown in Fig. 1(b). We admittedly agree that it may remain a rather long-range component in the data also after filtering. Certainly, we do not have enough data to capture all the nonlinear dynamics. Nevertheless, we can still have a low-dimensional chaotic dynamics for an inertial sub-manifold of the phase space, e.g., [2].

Table 1 summarizes the selected calculated characteristic of the detrended and smoothed data shown in Fig . 1(b). The probability distributions are clearly non-Gaussian, cf. [19], and show distinct skewness (the third moment) of ~ 0.45 (as compared with its normal standard deviation of approximately $(15/N)^{1/2} = 0.06$). However, kurtosis (the fourth moment) is still small (cf. the value of -0.17 in Table 1 with the underlying standard deviation of $(96/N)^{1/2} = 0.15$). Admittedly, normal distributions are not excluded for chaotic data but are usually typical for stochastic systems; on the other hand, there are stochastic systems showing non-Gaussian distributions. Therefore, we cannot expect that all the dynamics is given by the probability distributions.

Given the high sampling rate, the maximum (Nyquist) frequency is indicated in Table 1, with the minimum frequency $1/(N\Delta t)$. Here, rather than using a fast Fourier transform method, we use the maximum-entropy method, which represents the data in terms of a finite number of complex poles of discrete frequency and is good for extracting sharp, discrete lines from an otherwise noisy data record. As seen in Fig. 2(a), the solar wind spectral density, obtained using 32 poles, is broadband and has a continuous part without dominant frequencies (for $f > 5 \times 10^{-4}$ Hz, cf. Table 1 and, e.g., [12, upper inset to Fig. 1]). This part is approximately a straight line on a logarithmic-linear scale. Naturally, periodic or quasi-periodic data would produce only a few dominant peaks in the spectrum.

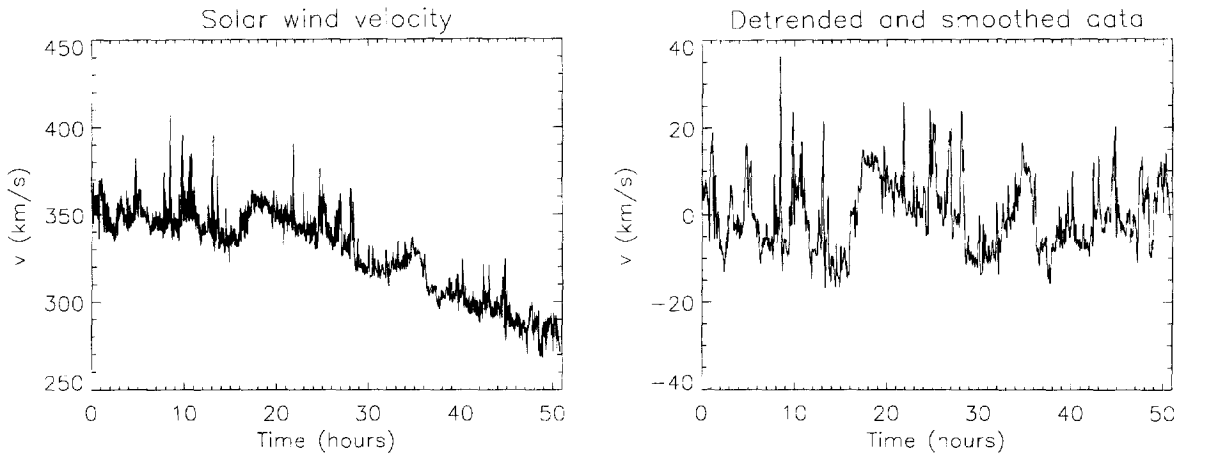

(a) (b)

Fig. 1. The radial velocity, v, observed by the Helios 1 spacecraft in 1975 from 67 : 08 : 20.5 to 69 : 11 : 07 (day : h : min) at distances 0.32 AU from the Sun, (a) the raw data, (b) the detrended and smoothed data.

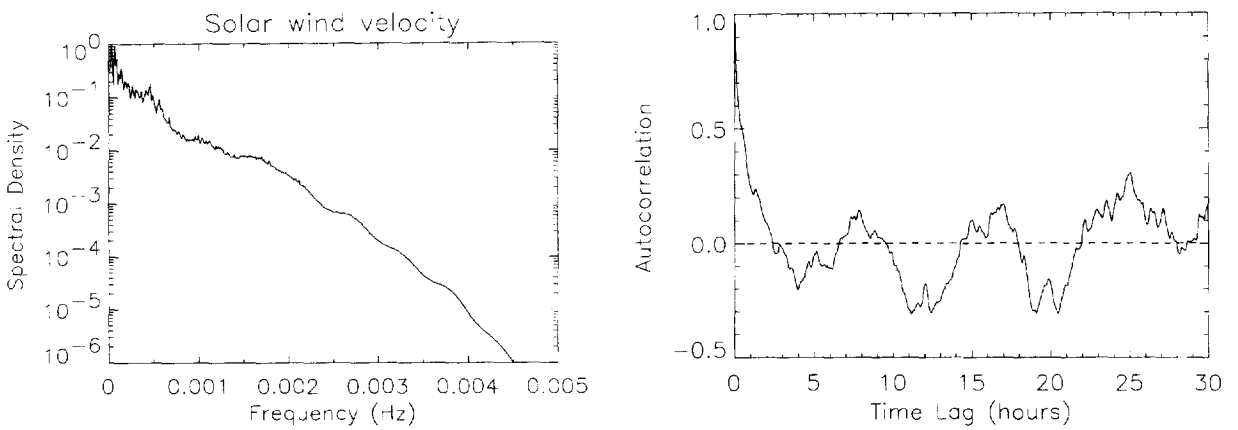

(a) (b)

Fig. 2. (a) The logarithm of spectral density (normalized) as a function of frequency, (b) the (normalized) autocorrelation function as a function of the time lag for the detrended and smoothed data.

In addition, we have estimated Lempel–Ziv measure of *complexity*, relative to white noise. The simplest coding is used: each data point is converted to a single binary digit according to whether its value is greater than or less than the median value, and the algorithm of Kaspar and Schuster [20] is used. The calculated value is rather small of ~ 0.2 (maximal complexity, or randomness, would have a value of 1.0, while a value of zero denotes perfect deterministic nonlinear predictability). This also indicates that the low-speed solar wind is a good candidate for chaos, but tells as yet nothing about a possibly *strange* attractor of the system.

3. Method

First, we briefly recall the standard method of the embedding space using singular-value decomposition developed in a basic paper by Broomhead and King

[21]. Albano et al. [22] have shown that combining singular-value decomposition and the Grassberger–Procaccia algorithm [16,18] can alleviate some of the ambiguities associated with each technique when used alone.

3.1. Embedding space

Using our time series of equally spaced, detrended and smoothed data, as shown in Fig. 1(b), we first construct the vectors $\mathbf{X}(t_i) = [v(t_i), v(t_i + \tau), \ldots, v(t_i + (m-1)\tau)]$ in the embedding phase space of dimension m.

We choose a time delay τ slightly larger than the autocorrelation time, see Table 1. This makes certain that $v(t)$ and $v(t+\tau)$ are at least linearly time independent, e.g., [5,23]. As shown in Fig. 2(b), the autocorrelation function first decreases by a factor $1/2$ in half an hour and then reaches zero at 2.4 h, cf. [12, a lower inset to Fig. 1] (see also Table 1). In fact, the autocorrelation time is still much smaller than the duration of the sample (50 h). We have tried longer samples, but in this case one should expect that nonstationarity would play a more important role. Therefore we prefer to study the shorter sample, which is still not bad, if the dimension of the attractor is well below $2 \log_{10} N \approx 7.3$ [24]. This is an optimal choice between the available number of measurement points and a very approximate stationarity. Admittedly, the number of vectors, $n = N - (m-1)\tau$, i.e., is decreasing with m and τ. Also the window length $\tau(m-1)$ becomes very large. But even for $m = 8$ and $\tau = 250\,\Delta t$ (after the first zero of the autocorrelation function) the number of vectors is equal to $n = 2764$, which is still not bad. For $m = 12$ the statistic is poorer, $n = 1764$, even though deterioration is weakened by the logarithmic dependence.

3.2. Singular-value decomposition

Using the normalized vectors $\mathbf{X}(t_i)$, where $i = 1, \ldots, n$, for each m-dimensional embedding space, we now consider A that is the $n \times m$ trajectory matrix $(n \geq m)$ [21,22]

$$A = \frac{1}{\sqrt{n}} \begin{pmatrix} \mathbf{X}(t_1) \\ \mathbf{X}(t_2) \\ \vdots \\ \mathbf{X}(t_n) \end{pmatrix}$$

The matrix $A_{ij} = v(t_i + (j-1)\tau)$ can be expressed as: $A = UWV^{\mathrm{T}}$, where U is an $n \times m$ matrix with orthonormal columns, $(U^{\mathrm{T}}U)_{ij} = \delta_{ij}$; V is an $m \times m$ orthonormal matrix, $(V^{\mathrm{T}}V)_{ij} = (VV^{\mathrm{T}})_{ij} = \delta_{ij}$; and W is an $m \times m$ diagonal matrix, $W_{ij} = \delta_{ij} w(j)$.

The elements of the diagonal matrix W are known as the *singular* values of A. The squares of the singular-values $w^2(i)$ are the eigenvalues of the covariance matrix, $A^{\mathrm{T}}A$, while the columns of V are its eigenvectors, with the directions called the *principal* axes. The projection of the original vectors onto the new orthogonal space is given by the transformation: $A \to A' = AV = UW$. Therefore, the rotated matrix A' is also called the matrix of principal components. The square of the singular value $w^2(i)$ is the variance of the ith principal component and can be interpreted as probability that the reconstructed trajectory 'visits' the ith principal axis.

In particular, if, for some k, $w^2(k) = 0$, then the trajectory does not visit the principal axis k. Basically, noise prevents any eigenvalue from vanishing. Hence by limiting the number of basic eigenvectors, by taking only those corresponding to some large eigenvalues, we remove a substantial amount of the inherent noise of the experimental data [21,22].

The normalized eigenvalues as a function of index, sorted from largest to smallest, for the detrended and smoothed solar wind data in Fig. 1(b) are displayed in Fig. 3 (boxes). For comparison, the eigenvalues for the data generated by the standard *Lorenz* equations using 2000 points at intervals of $\Delta t = 0.05$, $\tau = 5\Delta t$, are shown by stars. In both cases the largest value dominates the other eigenvalues. The eigenfunctions corresponding to the two largest eigenvalues, for the solar wind data are plotted versus time in Fig. 4. The largest eigenfunction corresponds to the dominant largest eigenvalue as is also the case in chaotic systems, e.g., for the very standard *Lorenz* system.

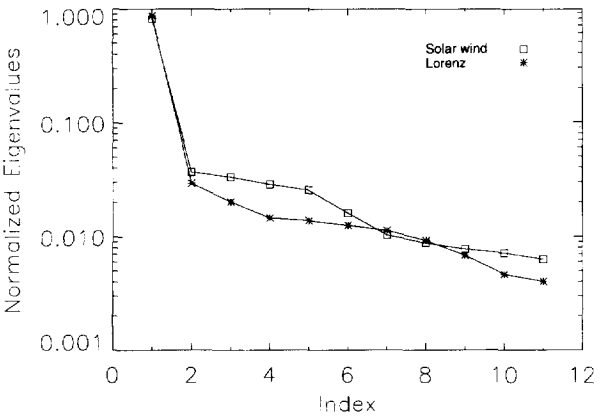

Fig. 3. Normalized eigenvalues ξ_i as a function of index for the detrended solar wind data in Fig. 1(b) (boxes) and, for comparison, for the data generated by the Lorenz equations using 2000 points at intervals of 0.05 (stars).

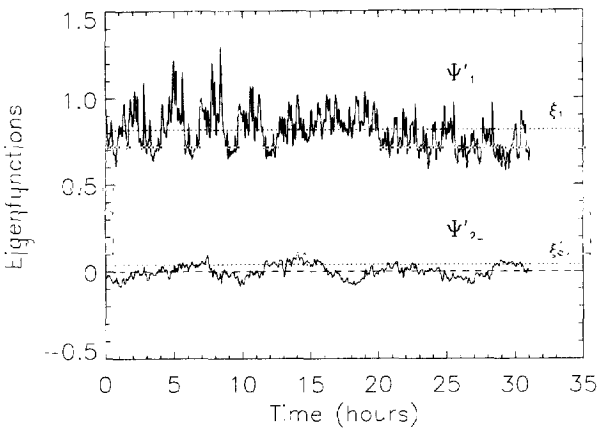

Fig. 4. The eigenfunctions, normalized for $m = 8$, corresponding to the two largest eigenvalues versus time for the solar wind data ($\psi' = A'W$).

4. Attractor reconstruction

First, we have tried to reconstruct the attractor, at least its projection onto three-dimensional subspace of the phase space, $[v(t), v(t+T), v(t+2T)]$, using a delay $T = 4\Delta t$ without using the method of singular-value decomposition. Obviously, for a periodic system we would have a simple closed loop. In our case (changing slightly T), we have a trajectory with a discernible quasi-loop structure, which is somewhat similar to the Rössler attractor, combined with another interesting spindle-shaped structure as shown for a selected perspective in Fig. 5(a).

Admittedly, spiral-like features are also present in systems that do not exhibit low-dimensional chaos. To test the topological properties of the reconstructed attractor we will invoke the method of singular-value decomposition [21,22]. In this method the data are represented in terms of a complete set of orthogonal functions, which is obtained from a numerical analysis of the data and is not imposed from outside, as in the Fourier series or wavelets representation.

If the attractor dimension is less than 4, as argued by Macek and Obojska [11–13], for embedding dimension ($m = 8$) satisfying the Takens embedding condition, we have verified that, in practice, even four eigenfunctions are sufficient to reproduce the nonlinear dynamics of the system. The attractor obtained using five largest eigenvalues (projected onto three principal empirical eigenvector $U(k) = \Psi_k$ (where $k = 1, 2, 3$) is shown in Fig. 5(b).

We have also studied how the topology of the attractor depends on the number of eigenvalues? In particular, we have always one largest eigenvalue corresponding the principal axis of the attractor, see Figs. 3 and 4. As compared with Fig. 5(a), the axis of the structure in Fig. 5(b) is rotated in phase space but the attractor is topologically similar. Obviously, the Euclidean distances are invariant under the rotation in the phase space and the embedding space, and the topological properties of both structure should also be similar.

5. Dimension and entropy

We now divide the m-dimensional embedding phase space into a large number of equal hypercubes of size r. Assume that $M(r)$ is the number of these cubes that are needed to cover the presumed attractor. If p_i is the probability measure that a point from a long time series falls in a typical ith hypercube, using the q-order function $I_q(r) = \sum(p_i)^q$, $i = 1, \ldots, M$, the generalized dimension is, e.g., [2,4,15,23]

$$D_q = \frac{1}{q-1} \lim_{r \to 0} \frac{\log I_q(r)}{\log r}. \tag{1}$$

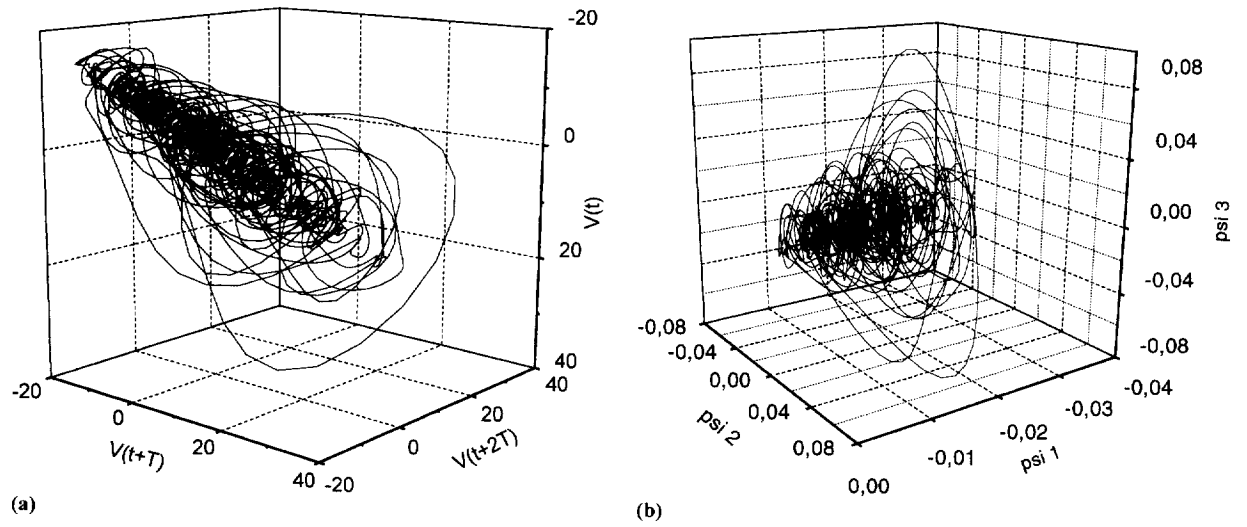

Fig. 5. The projection of the attractor onto the three-dimensional space, reconstructed from the detrended data, using (a) the moving average and also (b) the singular-value decomposition filters ($\psi = U$).

The related quantity $K_q = \lim_{r\to 0}[1/(1-q)] \log I_q(r)$, called the q-order *Kolmogorov entropy*, is the rate of creation of information as a chaotic orbit evolves [2,15,23].

We see from Eq. (1) that the larger q is, the more strongly are the higher probability cubes (visited more frequently by a trajectory) weighted in the sum for $I_q(r)$. Since the data cannot constrain well the capacity dimension D_0, we look for higher order dimensions, which quantify the multifractality of the probability measure on the attractor. In practice, $q = 2$ is sufficient and $I_2(r)$ is taken to be equal to the correlation function $C_m(r)$ given in Table 1, which is calculated using the Grassberger and Procaccia [16,18] algorithm.

The procedure of singular-value decomposition by itself cannot change the dimension because it is simply the rotation in the embedding space. If we keep all eigenvalues, this result is exact, because rotation preserves the distances used in the calculation of the correlation function $C_m(r)$. Naturally, by limiting to most probable eigenvalues we change slightly the distances. But it was proven that one automatically removes some noise. The theory guarantees that the correlation dimension can be calculated as long as the number of eigenvalues kept is greater than the dimension [15,21].

We follow Albano et al. [22], as discussed in Section 3. Namely, for a given embedding m, a singular-value decomposition is performed, yielding the matrix of singular-values W, and the orthogonal matrices V and U. The trajectory matrix A is rotated, by replacing A by U (they are of the same size) and multiplying by the matrix of singular-values W, i.e., $A' = UW$. The resulting matrix of principal components, A', is then used in a Grassberger–Procaccia calculation. It is essential that now only several *large* singular values (above the noise level) can be taken in W, while the smaller are replaced by zeros.

6. Results and discussion

We calculate the correlation function $C_m(r)$, as discussed in Section 5 and Table 1, versus log r (normalized) for various embedding dimensions: $m = 4$ (dotted curve), $m = 5$ (diamonds), 6 (triangles), 7 (squares), and 8 (crosses). The results obtained without using singular-value decomposition, or equivalently taking all eigenvalues, are presented in Fig. 6(a). The corresponding slopes of the natural logarithm of the correlation functions $\mathrm{d}(\log C_m(r))/\mathrm{d}(\log r)$

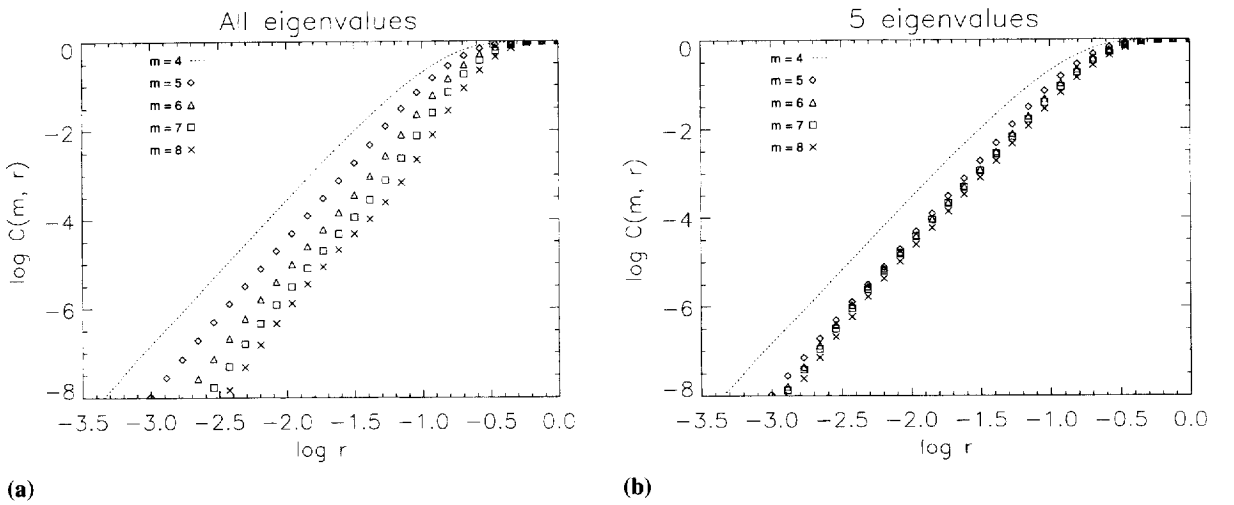

Fig. 6. The correlation function $C_m(r)$ versus $\log r$ (normalized) is shown for various embedding dimensions: $m = 4$ (dotted curve), $m = 5$ (diamonds), 6 (triangles), 7 (squares), and 8 (crosses). (b) Similarly, the correlation function obtained using the singular-value decomposition with five largest eigenvalues.

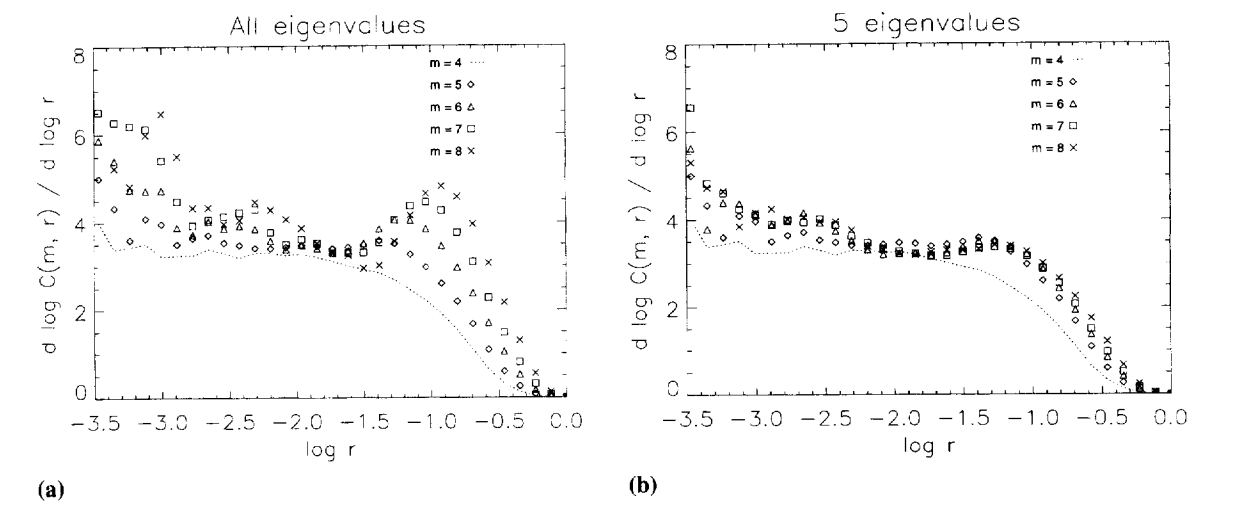

Fig. 7. (a) The slope, $\mathrm{d}(\log C_m(r))/\mathrm{d}(\log r)$, of the correlation function $C_m(r)$ versus $\log r$ (normalized) is shown for various embedding dimensions: $m = 4$ (dotted curve), $m = 5$ (diamonds), 6 (triangles), 7 (squares), and 8 (crosses). (b) Similarly, the slope obtained using the singular-value decomposition with five largest eigenvalues.

are shown in Fig. 7(a). Admittedly, due to the necessarily finite amount of data, the range of r with the meaningful plateau is limited to $-3 < \log r < -1$. At small r this plateau is smeared out by statistical fluctuations in determining p_i in Eq. (1), and at large r – by the size of the attractor, e.g., [2]. Similarly, the results obtained using singular-value decomposition taking five largest eigenvalues are given in Fig. 6(b) and the corresponding slopes are shown in Fig. 7(b). If the D-dimensional attractor exists, we expect a plateau for $m \geq D$ [25,26] (dotted curve) and in the worst case for $m > 2D$ [3]. Comparison of Figs. 7(a) and (b) shows that a better plateau is obtained by using the singular-value decomposition technique

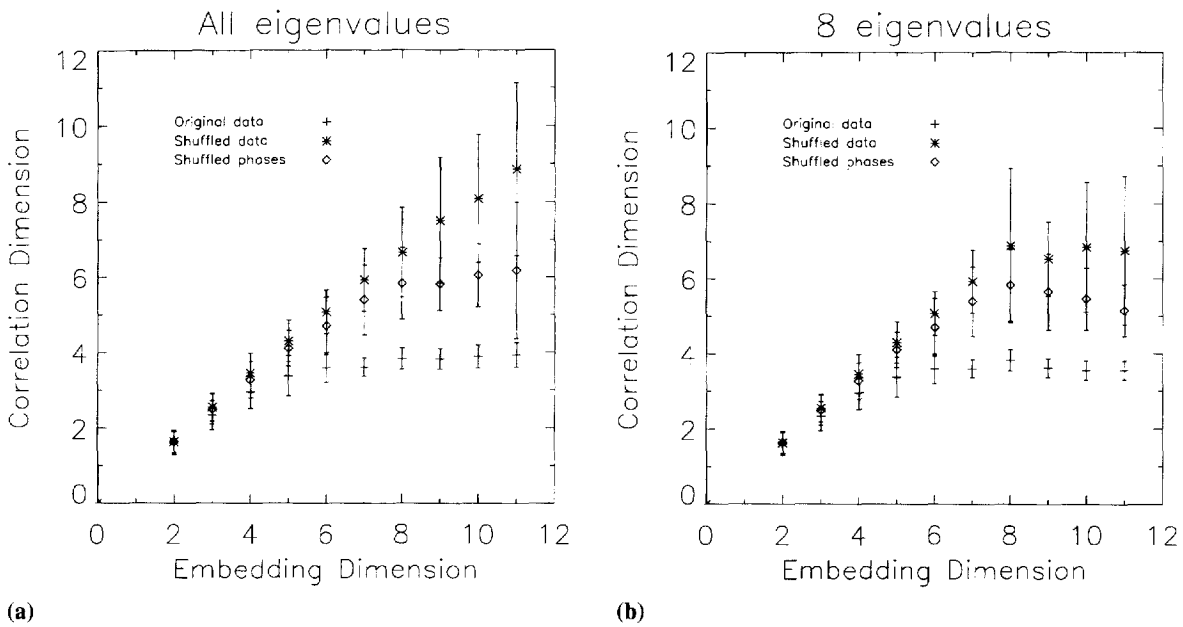

Fig. 8. The correlation dimension (slope), D_2, as a function of the embedding dimension m (for $m = 2, \ldots, 12$) obtained using (a) the moving average and (b) the singular-value decomposition filters are shown by plus signs with error bars. The average slope for $6 \leq m \leq 10$ yields $D_2 = 3.7 \pm 0.3$. The calculated values of D_2 for surrogate data [29] with the same probability distribution or the same SPECTRUM and the autocorrelation but with the *determinism removed* from the original data are shown by asterisk or DIAMOND signs, respectively, cf. e.g., [27, Fig. 19(b)], and [29, Fig. 7(a)].

of noise reduction. This proves that this powerful method is more adequate than simple moving average smoothing, especially in the case of an underlying low-dimensional attractor.

Basically, the embedding method can, in principle, distinguish the chaotic deterministic behaviour from the white noise, e.g., [27]. The noise fills-up any available m-dimensional phase space, while the calculated dimension levels off for the deterministic chaotic system. Namely, as we increase the embedding dimension, the computed *correlation dimension*, D_2, saturates at some finite value of m, but keeps increasing for a stochastic system.

For m large enough a plateau in the scaling region indicates a proper correlation dimension D_2. We see a clear plateau which appears already for $m = 4$ and 5, cf. [11–13]. For higher dimensions, $m \geq 8$, the plateau is still present but more smeared out by the statistical fluctuations at small r. We have extended our calculations for embedding space of dimension as large as $m = 16$. However, because for $m = 16$ the statistic is very poor ($n = 764$), we do not consider the calculations for $m > 10$ very seriously. The average slope for $6 \leq m \leq 10$ yields $D_2 = 3.7 \pm 0.3$. The inferred correlation dimension (*slope*), D_2, as a function of the embedding dimension (for $m = 2, \ldots, 12$) is shown as plus signs in Fig. 8(a) for moving average and in Fig. 8(b) for moving average and singular-value decomposition filters. The error bars in Figs. 8(a) and (b) are obtained assuming normal distribution of the rms errors over the best scaling range. In both cases the slope of the calculated correlation function saturates for $m > 5$; this is consistent with the attractor of the low-dimension, between 3 and 4, cf. [28].

The obtained measures of the inferred attractor have been subjected to the surrogate data test [29]. First, we consider the question whether there is evidence for any dynamics at all. In this case the null hypothesis is that the observed data are fully described by independent and identically distributed random

variables. To test this hypothesis we generate surrogate data by shuffling the time-order of the original time series. In this way any temporal correlations are destroyed in the data. Second, another null hypothesis is that all the structure in the original time series is given by the Fourier spectrum (or equivalently by the autocorrelation function). In this case we Fourier-transform the data, randomize the phases, and then inverse Fourier-transform the results to get a new time series.

In both cases, if the original data are indeed deterministic, analysis of these surrogate data, after removing possible deterministic *nonlinearities*, will provide values that are statistically distinct from those derived for the original data. Again, the results obtained without and with using singular-value decomposition are presented in Figs. 8(a) and (b), correspondingly. Here we also show the correlation dimension calculated for each embedding dimension m for surrogate simply shuffled data (`asterisk` signs). This operation preserves the probability `distribution` but generally produces a very different power spectrum and the autocorrelation function. The operation using shuffled phases, on the contrary, gives the same SPECTRUM and the autocorrelation function but generally produces a different probability distribution. These results are shown by DIAMONDS. For these two upper curves in Fig. 8(b) (shuffled cases) we have now taken eight eigenvalues, so consequently the calculated points for $m > 8$ are underestimated. Finally, even though the actual errors in Figs. 8(a) and (b) could be somewhat larger than adopted, the statistical significance of the difference of these curves from that obtained using the original data is clear. This decidedly demonstrates that our original data (a lower curve, plus signs) are significantly different from noise, cf. e.g., [27, Fig. 19(b); 29, Fig. 7(a)].

Moreover, like eigenvalues of a linear system, Lyapunov exponents quantify a nonlinear system's stability in various directions. The *chaotic attractor* has at least one unstable direction, i.e., at least one positive exponent, yet the overall system is stable, i.e., the sum of all Lyapunov exponents is *not* positive. We only calculate the largest positive Lyapunov exponent $\lambda_{\max}$ using the algorithm of Wolf et al. [30]. We obtain the magnitude of 1/4 to 1/3 in units of bits (factor of 2) per data sample. In general, the entropy K_q is at most the sum of the positive Lyapunov exponents $\sum \lambda_i$, e.g., [2,15]. As shown in Table 1, the value of the Lyapunov exponent is consistent (within a factor of 2) with the Kolmogorov correlation ($q = 2$) entropy [18] $K_2 \sim 1/3$ (base 2), which should be its lower bound: $K_2 \leq \sum \lambda_i$. The time over which the meaningful prediction of the behaviour of the system is possible is roughly $\sim 1/\lambda_{\max}$, e.g., [1]. Hence the predictability of the system is limited to about 1 h.

Finally, we have found that the nonlinear deterministic system is sensitive to the surrogate-data test, contrary to the stochastic system. In particular, as compared with the quantities listed in Table 1, the largest Lyapunov exponent (and entropy) increases by a factor of 3, and Lempel–Ziv complexity calculated for shuffled-data becomes clearly 1.0, as it should be for a purely stochastic system.

7. Conclusions

We have shown that the probability distribution of the velocity fluctuations of the solar wind in the inner heliosphere is non-Gaussian. The spectrum is broadband and has a continuous part that reveals aperiodic behaviour of the flow. The autocorrelation function falls to zero in a finite time. Further, the calculated measure of algorithmic *complexity*, relative to white noise, is rather small of ~ 0.2. The system is likely to have an attractor lying in the inertial manifold of low-dimension (less than 4). The *entropy* and the largest *Lyapunov* exponent are positive implying sensitive dependence on initial conditions. Hence we suggest that there exists an inertial manifold for the low-speed solar wind in the inner heliosphere, in which the system is *nonlinear* and possibly deterministic chaotic, and where noise is certainly not dominant. This means that the observed irregular and turbulent behaviour of the velocity fluctuations results rather from intrinsic nonlinear chaotic dynamics than from random external forces.

Acknowledgements

This work was supported by the State Scientific Research Committee Grant 2P03C 012 10. The author thanks A.W. Wernik for a fundamental numerical program for calculating the fractal dimension and L. Obojska for help in preparation of some of the figures. He is also grateful to H. Rosenbauer for introducing the Helios data to him and to J.A. Yorke and C. Grebogi for stimulating discussions. Some characteristics in Table 1 were obtained using Chaos Data Analyzer (the professional version) by J.C. Sprott and G. Rowlands.

References

[1] S.H. Strogatz, Nonlinear Dynamics and Chaos, Addison-Wesley, Reading, MA, 1994.
[2] E. Ott, Chaos in Dynamical Systems, Cambridge University Press, Cambridge, 1993.
[3] F. Takens, Detecting strange attractors in turbulence, in: D.A. Rand, L.S. Young (Eds.), Lecture Notes in Mathematics, vol. 898, Springer, Berlin, 1981, pp. 366–381.
[4] T. Sauer, J.A. Yorke, M. Casgali, Embedology, J. Stat. Phys. 65 (1991) 579–616.
[5] H.D.I. Abarbanel, R. Brown, J.J. Sidorowich, L.S. Tsimring, The analysis of observed chaotic data in physical systems, Rev. Modern Phys. 65 (1993) 1331–1392.
[6] J. Kurths, H. Herzel, An attractor in a solar time series, Physica D 25 (1987) 165–172.
[7] N.O. Weiss, Chaotic modulation of the solar cycle, Philos. Trans. R. Soc. A 348 (1994) 445–447.
[8] D.V. Vassiliadis, A.S Sharma, T.E. Eastman, K. Papadopoulos, Low-dimensional chaos in magnetospheric activity from AE time series, Geophys. Res. Lett. 17 (1990) 1841–1844.
[9] D.A. Roberts, Is there a strange attractor in the magnetosphere?, J. Geophys. Res. 96 (1991) 16031–16046.
[10] R. Schwenn, Large-scale structure of the interplanetary medium, in: R. Schwenn, E. Marsch (Eds.), Physics of the Inner Heliosphere, vol. 20, Springer, Berlin, 1990, pp. 99–182.
[11] W.M. Macek, L. Obojska, Fractal analysis of the low-speed solar wind flow, in: A. Hilgers, T.-D. Guyenne (Eds.), ESA Symposium Proceedings on Environment Modelling for Space-based Applications, SP-392, ESTEC, Noordwijk, December 1996, pp. 247–252.
[12] W.M. Macek, L. Obojska, Fractal analysis of the solar wind flow in the inner heliosphere, Chaos, Solitons and Fractals 8 (1997) 1601–1607.
[13] W.M. Macek, L. Obojska, Testing for nonlinearity in the solar wind flow, in: T. Kapitaniak, J. Brindley (Eds.), Proceedings of Third International Conference on Applied Chaotic Systems, Chaos, Solitons and Fractals 9 (1998) 221–229.
[14] R. Badii, G. Broggi, B. Derighetti, M. Ravani, S. Ciliberto, A. Politi, M.A. Rubio, Dimension increase in filtered chaotic signals, Phys. Rev. Lett. 60 (1988) 979–982.
[15] E. Ott, T. Sauer, J.A. Yorke, Coping with Chaos, Wiley, New York, 1994.
[16] P. Grassberger, I. Procaccia, Measuring the strangeness of strange attractors, Physica D 9 (1983) 189–208.
[17] J. Theiler, Spurious dimension from correlation algorithms applied to limited time-series data, Phys. Rev. A 34 (1986) 2427–2432.
[18] P. Grassberger, I. Procaccia, Estimation of the Kolmogorov entropy from a chaotic signal, Phys. Rev. A 28 (1983) 2591–2593.
[19] E. Marsch, C.Y. Tu, Non-Gaussian probability distributions of solar wind fluctuations, Ann. Geophys. 12 (1994) 1127–1138.
[20] F. Kaspar, H.G. Schuster, Easily calculable measure for the complexity of spatiotemporal patterns, Phys. Rev. A 36 (1987) 842–848.
[21] D.S. Broomhead, G.P. King, Extracting qualitative dynamics from experimental data, Physica D 20 (1986) 217–236.
[22] A.M Albano, J. Muench, C. Schwartz, A.I. Mess, P.E. Rapp, Singular-value decomposition and the Grassberger–Procaccia algorithm, Phys. Rev. A 38 (1988) 3017–3026.
[23] H.G. Schuster, Deterministic Chaos, VCH, Weinheim, Germany, 1989.
[24] J.-P. Eckmann, D. Ruelle, Fundamental limitations for estimating dimensions and Lyapunov exponents in dynamical systems, Physica D 56 (1992) 185–187.
[25] M. Ding, C. Grebogi, E. Ott, T. Sauer, J.A. Yorke, Plateau onset for correlation dimension: When does it occur? Phys. Rev. Lett. 70 (1993) 3872–3875.
[26] T. Sauer, J.A. Yorke, How many delay coordinates do you need?, Int. J. Bifurcation Chaos 3 (1993) 737–744.
[27] J. -P. Eckmann, D. Ruelle, Ergodic theory of chaos and strange attractors, Rev. Mod. Phys. 57 (1985) 617–656.
[28] E. Marsch, S. Liu, Structure functions and intermittency of velocity fluctuations in the inner solar wind, Ann. Geophys. 11 (1993) 227–238.
[29] J. Theiler, S. Eubank, A. Longtin, B. Galdrikian, J.D. Farmer, Testing for nonlinearity in time series: The method of surrogate data, Physica D 58 (1992) 77–94.
[30] A. Wolf, J.B. Swift, H.L. Swinney, J.A. Vastano, Determining Lyapunov exponents from a time series, Physica D 16 (1985) 285–317.